Analysis and design of wedge transducers using the boundary element method

Guillermo Rus and Shi-Chang Wooh[a)]
NDE Lab, Department of Civil and Environmental Engineering, Massachusetts Institute of Technology, Cambridge, Massachusetts 02139

Rafael Gallego
Department of Structural Mechanics, University of Granada, Spain

(Received 14 June 2003; accepted for publication 5 December 2003)

Cones or wedges inserted between an ultrasonic transducer and a specimen enhances certain characteristics of the transducers. Such an arrangement is useful in that the transducer can be used for transmitting and receiving signals on a point (or line) source, which can eliminate the undesirable aperture effect that makes the transducer blind to waves traveling in certain directions and to those of certain frequencies. In this paper, a comprehensive numerical analysis based on a wave propagation model is carried out to study the characteristics and parameters of wedges. We study the effect of dimensions, shape and aperture on frequency response and directivity. For computational accuracy and efficiency, the boundary element method is used in the analysis. [DOI: 10.1121/1.1737738]

Pages: 2919–2927

PACS numbers: 43.38.Fx, 43.38.−p, 43.35.Yb [JGH]

I. INTRODUCTION

Ultrasonic transducers used in the non-destructive evaluation (NDE) and testing (NDT) are traditionally fabricated in circular or rectangular shapes of finite dimensions (typically 0.5 to 2.5 cm diameter). Although these transducers are easy to manufacture and they provide strong and well-directed signals, there are some disadvantages associated with their relatively large dimensions with respect to the wavelengths. The main disadvantages of a large transducer include signal distortion, the fact that certain frequency components may be cut off, and the near field effect, which are generally referred to as *aperture effects*.

The benefits of using point sources and point receivers for NDE have been addressed by Sachse.[1] One of the ways to produce point contact between the transducer and the target surface is to use a miniature or pencil-tip transducer. Lee *et al.*[2] demonstrated a technique to achieve small contact surface areas of as low as 200 to 400 μm in diameter by directly cutting a piezoelectric plate using a laser beam. Another and perhaps easier way to provide point contact is to use a cylindrical cone or a triangular wedge whose vertex or knife-edge is in contact with the surface while a normal sized transducer is mounted on the flat surface of the wedge. Note that the former (cone) produces a point contact while the latter (wedge) can be used to produce a hairline contact. The use of wedges to collimate waves and to generate point sources was first introduced by Ying in 1967.[3]

The propagation of ultrasonic waves radiating from a transducer has been studied by many investigators in an effort to understand the response of the transducer as a system. For example, Imamura[4] computed the particle velocities of the waves for circular point transducers. Kimoto and Hirose[5] studied a transmitter–receiver setup by modeling the transmitting transducer as a distributed traction and using a weight function on the displacements of the receiving transducer. They used the boundary element method (BEM) to model the pulse-echo test from a standard A-scan signal. To improve the model of the transducer, Schmerr[6] introduced the transfer function for the transducer–specimen system, which makes it possible to obtain variations of approximately 20% between the experimental and numerical signals. Marty *et al.*[7] experimented with the propagation of Lamb waves generated by point source excitation on the surface of a plate. Wooh and Zhou[8,9] and Shi and Wooh[10,11] studied the behavior of laser excited ultrasonic bulk and guided waves, respectively. A general guideline to design transducers can be found in the Nondestructive Testing Handbook.[12] Note that these are just a few examples of the many studies previously carried out.

Despite the abundance of studies in these areas and the fact that wedges have been used in practice for a long time, the response of the wedge has not been studied in great detail. To our understanding, little knowledge about the effect of mechanical coupling between the transducer and the specimen through a wedge is available. The study described in this paper is motivated by the capacity of point or hairline transducers to overcome the deletérious aperture effects of larger transducers. We report the results of a comprehensive parametric study in an effort to establish guidelines and criteria for optimum wedge design. The conclusions drawn from our numerical study allow us to predict the influences of boundary conditions and wedge geometries on the transducer–specimen coupling mechanisms.

II. TRANSDUCER DESIGN ASPECTS

A. Aperture effects

To demonstrate the aforementioned aperture effects, we take the example of a large transducer used in detecting Rayleigh waves on the surface. The response of the transducer

[a)]Send correspondence to Professor Shi-Chang Wooh, 5 Moore Cir., Bedford, Massachusetts 01730. Electronic mail: scwooh@mit.edu

TABLE I. Design criteria.

Criteria	Effect
Small contact area with specimen	Reduces the aperture effect.
Large contact area with specimen	Can transmit higher energy.
Large contact area with transducer	Can transmit higher energy.
Wedge shape	Avoids spurious eigen-modes or unexpected wave propagations (within the wedge in comparison to direct contact). Allows for feasible manufacturing processes.

can be expressed by the superposition of the wave displacements detected by the transducer as the wave propagates through the surface of contact between the transducer and the target material, that is,

$$u(t)=\frac{1}{A}\int_{\Omega}u(\mathbf{x},t)d\Omega, \tag{1}$$

where $u(t)$ is the surface displacement and Ω is the contact surface of the area A. If a one-dimensional harmonic wave of the form

$$u(x,t)=B\cos(kx-\omega t), \tag{2}$$

is considered to be detected by a circular transducer of radius a, where k is the wave number and ω is the angular frequency, then the detected signal would be expressed in the simple form

$$u(t)=\frac{2J_1(ka)}{ka}B\cos(\omega t), \tag{3}$$

whose amplitude has zero-crossing points at every root of the Bessel function $J_1(ka)$.

B. Design criteria

As explained earlier, the problem of the vanishing frequency components due to phase cancellation can be resolved by physically reducing the size of the contact area using a wedge. An optimal design can be reached by considering the effects shown in Table I. Our goals are to optimize the design based on manufacturing and operation criteria while maintaining the simplicity of signal transmission and reducing the aforementioned oscillatory effects.

III. SYSTEM RESPONSE

A. Transfer function

In order to characterize the transducer–specimen wedge system, we use the transfer function, assuming that the system is linear time-shift invariant. Transfer functions are often expressed in terms of Green's functions when averaging the measurement over the transducer's surface area.

Our objective is to analyze the performance of the wedge working as a participating component of a complete NDE measurement system. A wedge can be used either as a transmitter or receiver, or both at the same time. For this, it is arguably sufficient that we only need to study the frequency response of transducers located at two well-chosen points. We first define a number of essential components of a typical ultrasonic NDE system shown in Fig. 1. The system consists of five distinct components characterized by their respective transfer functions denoted by the symbols $h^{(IT)}$ (function generator or pulser), $h^{(TP_i)}$ (transmitting transducer), $h^{(PU)}$ (specimen), $h^{(UR)}$ (receiving transducer), and $h^{(RO)}$ (signal receiving unit). In this system, we deal with four different signal levels: $s^{(I)}$ (input signal), $s^{(O)}$ (output signal), $s^{(T)}$ (signal just emitted from the transmitting transducer), and $s^{(R)}$ (signal arrived at the receiving transducer).

The electrical and mechanical responses of a transmitting transducer are invariants that can be determined independently by choosing the wedge parameters. Thus, the transmitted signal $s^{(T)}$ is defined simply as normal stresses or tractions distributed on the area of contact between the wedge and the transducer. The function $h^{(TP)}$ relates the emitted signal and the pressure induced in the specimen at an internal point z_2 located underneath the tip of the transmitting transducer, i.e.,

$$p(z_2)=h^{(TP)}*s^{(T)}. \tag{4}$$

The function $h^{(UR)}$ relates the received signal $s^{(R)}$ and the induced displacement $u(z_1)$ at a point (z_1) located underneath the receiving wedge, i.e.,

$$s^{(R)}=h^{(UR)}*u(z_1). \tag{5}$$

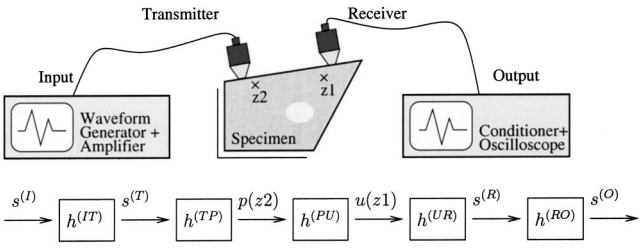

FIG. 1. Schematic of a generic NDE system.

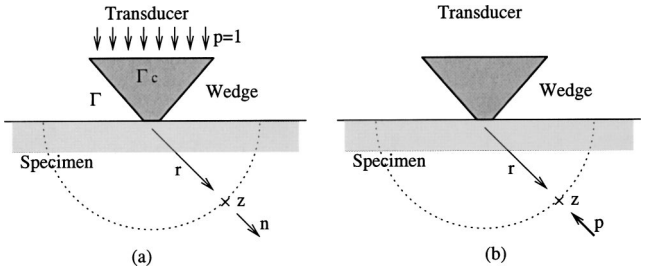

FIG. 2. Definitions of two reciprocal problems: (a) Transmitter and (b) receiver.

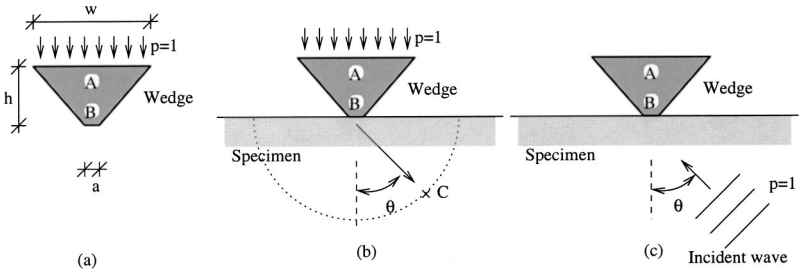

FIG. 3. Three different models used in the wedge design: Models (a), (b), and (c).

Likewise, the function $h^{(PU)}$ is the transfer function of the specimen relating u and p,

$$u(z_1)=h^{(PU)}*p(z_2), \tag{6}$$

which is also an invariant for different wedges. The transfer functions can be obtained directly in the transformed frequency domain by dividing the output signal by the input function. Similarly, $h^{(IT)}$ and $h^{(RO)}$ reflect the response of the two electrical systems of the transmitter, $s^{(T)}=h^{(IT)}*s^{(I)}$, and the receiver, $s^{(O)}=h^{(RO)}*s^{(R)}$.

The overall output of the system is the convolution of the input signal and the transfer functions of all the components in the signal path, i.e.,

$$s^{(O)}=s^{(I)}*h^{(IT)}*h^{(TP)}*h^{(PU)}*h^{(UR)}*h^{(RO)}. \tag{7}$$

Since the functions $h^{(IT)}$, $h^{(PU)}$, and $h^{(RO)}$ remain invariant through a test in regard to the wedge design, it is only necessary to study the functions $h^{(TP)}$ and $h^{(UR)}$, whose responses vary for different wedges. We use a partial model of the latter as follows.

B. Reciprocity between the transmitting and receiving subsystems

In principle, we should consider the wedges as integrated parts of the transmitting and receiving transducers. The transmitting wedge–specimen system model is shown in Fig. 2(a), in which the piezoelectric transducer is simply modeled as pressure distributed uniformly on the contact area Γ_c. Using this model, we can compute the particle displacements in the radial direction (**n**) at all the points z located on an arbitrary arc of fixed radius r. This allows us to study the directional dependency or the *directivity* of the waves propagating into the medium. To study the characteristics of the receiver assembly, a reciprocal model shown in Fig. 2(b) is considered. In this model, the particles on the arc of radius r are loaded in the **n** direction by applying pressure in the form of a Dirac delta function. Then, the output signal is calculated by integrating the normal displacements over the surface (Γ_c) of contact between the wedge and the receiving transducer.

It is sufficient to study only one of these models to analyze both cases, because the reciprocal model yields identical results. To prove this, we simply need to recall Betti's reciprocal theorem of continuum mechanics (Green's theorem) between the primary (a) and secondary (b) states, i.e.,

$$\int_\Omega b_k^b u_k^a\,d\Omega+\int_\Gamma p_k^b u_k^a\,d\Gamma=\int_\Omega b_k^a u_k^b\,d\Omega+\int_\Gamma p_k^a u_k^b\,d\Gamma, \tag{8}$$

where b_k is the body force field, u_k is the displacement field in the Ω domain, and $p_k=\sigma_{jk}n_j$ is the stress vector on the boundary Γ, respectively. If we apply the reciprocity theorem between the two states shown in Fig. 2 with the following loading and boundary conditions:

$$\text{Primary state (a)}\quad \begin{cases} b_k^a=0, \\ p_k^a=\begin{cases} (0,1), & \Gamma_c, \\ 0, & \text{elsewhere}, \end{cases} \end{cases} \tag{9}$$

$$\text{Secondary state (b)}\quad \begin{cases} b_k^b=\delta(z)n_k, \\ p_k^b=0, \end{cases} \tag{10}$$

then we get

$$n_k u_k^a(z)=\int_{\Gamma_c} u_2^b\,d\Gamma. \tag{11}$$

This means that the results of the two models are identical, and we need to study only one of the models to describe both.

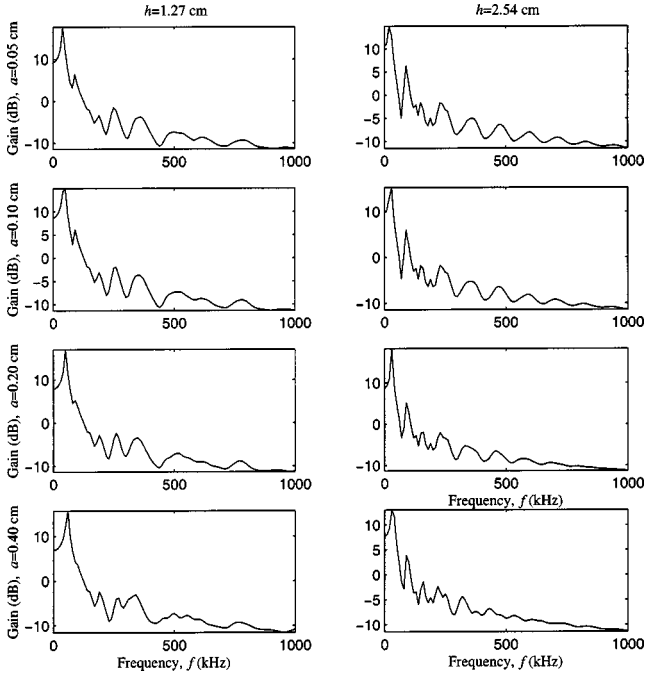

FIG. 4. Frequency response of the stocky (height=1.27 cm) and tall (height=2.54 cm) wedges with various contact areas. A wider and smoother plateau appears at high frequencies as a increases, particularly for the taller wedge.

TABLE II. Specifications of the wedge shapes considered in design.

Design	Profile	Contact area a (cm)	Height h (cm)	Focal frequency f_c (kHz)
1	Constant (no reduction of area)	2.540	0.000	0
2	Linear (narrow contact area)	0.010	1.270	489
3	Linear	0.100	1.270	489
4	Linear (wide contact area)	0.500	1.270	489
5	Linear (doubled height)	0.100	2.540	979
6	Linear (4×height)	0.100	5.080	1957
7	Linear (20×height)	0.100	25.400	9790
8	Linear (45 degrees sides)	0.100	1.220	470
9	Circular (concave: 0°–45°)	0.100	2.950	1136
10	Elliptical (vertically scaled×0.5)	0.100	1.470	566
11	Logarithmic ($y=a\log(bx)$)	0.100	1.270	489
12	Circular (convex)	0.100	1.260	485

C. Boundary element method

In studying and designing the wedge–specimen systems, we use the boundary element method (BEM) because of its clear advantages over the finite element or other discrete methods. First, the BEM does not require remeshing of the body domain at each iteration. This not only reduces the computational time but also eliminates small but important perturbations caused by changing the mesh. Second, by reducing the dimension of the problem by one, the fine meshes required by high frequency become affordable through the BEM.

We use the singular formulation of the boundary integral equation,

$$c_k^i(\mathbf{x})u_k(\mathbf{x}) + \int_\Gamma [p_k^i(\mathbf{y};\mathbf{x})u_k(\mathbf{y}) - u_k^i(\mathbf{y};\mathbf{x})p_k(\mathbf{y})]d\Gamma(\mathbf{y}) = 0.$$

This equation obviously relates the displacements u_k and the tractions p_k exclusively at the boundaries. If we use the complex presentation of fundamental harmonic solutions for p_k^i and u_k^i, then solving this equation yields fundamental harmonic solutions for a single frequency ω. In the equation, c_k^i is a geometry-dependent constant, and the integral has the sense of Cauchy's Principal Value. In implementation, we use the classical conforming discretization scheme with quadratic elements, eight-point Gauss integration after regularization and displaced collocation strategy. The implementation details are developed in Rus.[13] This equation is used for both boundary and internal points.[14,15]

IV. NUMERICAL RESULTS

The parametric design is based on three different models shown in Fig. 3. The model (a) shows an emitting transducer sitting on a standalone wedge. This model is used to study the effects of the transducer's contact areas and height. Model (b) shows the transmission of energy into the specimen through a wedge. This model is used to compute the transfer function of the combined assembly and directivity analysis. Finally, model (c) shows a signal coming from the specimen to the transducer mounted on a wedge. This model is used to demonstrate the improved reception due to the presence of the wedge. In addition, a combination of the models is used to analyze the effects of the boundary conditions.

To ensure the precision of the BEM results, the model was discretized with approximately 70 quadratic elements

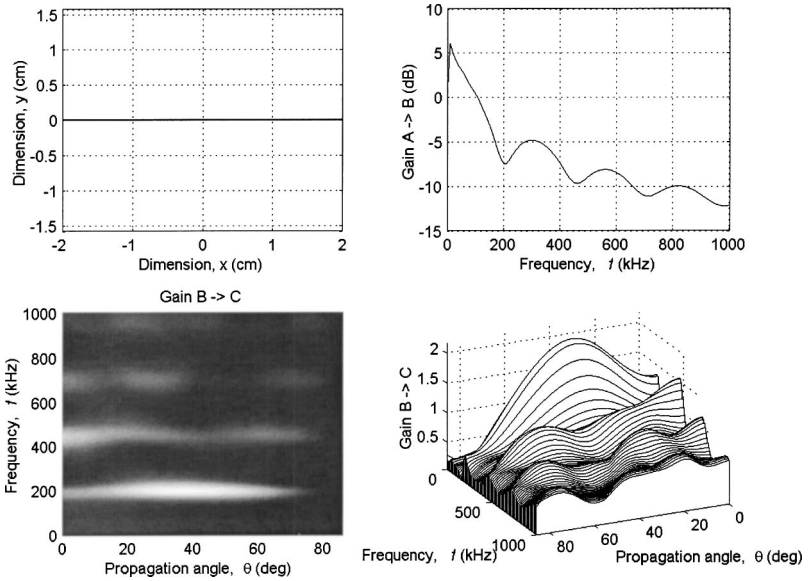

FIG. 5. Design 1. Combined frequency and directivity. Above left: wedge shape (no wedge), Above right: gain from zone *A* (transducer) to *B* (contact zone), Below: two perspectives of the gain from *B* to *C* (internal point in the specimen at every angle). Both gains should ideally be as horizontal and uniform as possible. Direct transducer–specimen contact (no wedge) gives undesirably wavy response in both frequency and directivity, as expected.

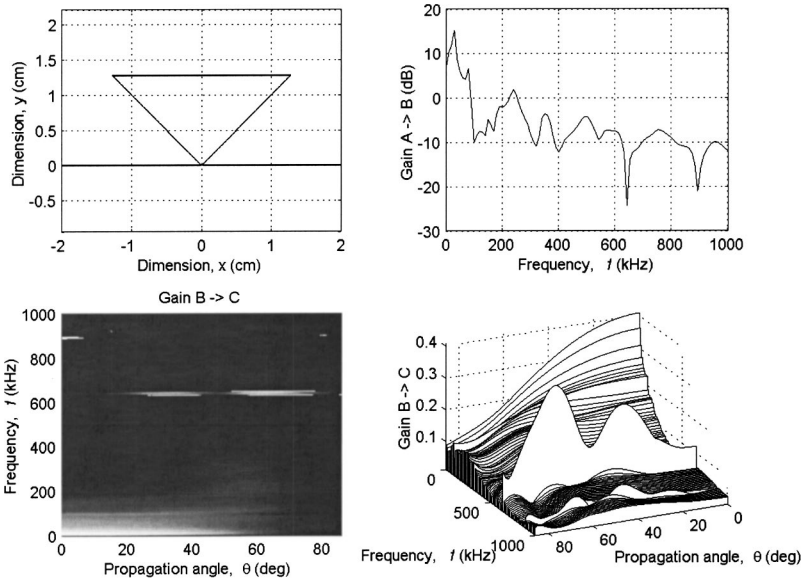

FIG. 6. Design 2. An ideally narrow contact area gives very flat directivity response in the high frequency band but with high signal attenuation. Design 3 (graphics omitted). A slightly enlarged contact area provides better results than those of Design 2.

and with a frequency sampling between 0 and 1 MHz at an increment of 10 kHz. The material used in this study is 4340 steel. The acoustical and physical properties of the material are given by its longitudinal wave speed $c_L = 5850$ m/s, transverse wave speed $c_T = 3240$ m/s and its mass density $\rho = 7220$ kg/m^3.

For the sake of convenience and without losing generality for conclusions, we only considered two-dimensional problems, in that a wedge was assumed to have an infinitely large dimension in its lateral direction. From the practical point of view, we use a fixed value of 2.54 cm (1.0 in.) for the dimension w (the area of contact between the transducer and the wedge). Then we varied the height (h) and the base contact area (a) of the transducer to study their influences on the transfer function.

A. Base contact area and height

Figure 3(a) illustrates the model of the isolated wedge with all free boundary conditions. In order to compute the transfer function of this model, we first consider a continuous monochromatic traction of unit magnitude applied on the transducer–wedge interface. Then the displacements at the bottom face (no traction) at all discrete locations are computed using the BEM, and they are integrated over the area to obtain the overall time-averaged output of the system. The ratio of the integrated displacement and the excitation function in the frequency domain yields the transfer function of the wedge.

To study the effects of the base contact area and the wedge height, we consider wedges of two slenderness ratios: stocky and tall wedges. Figure 4 shows the computed transfer functions of the stocky ($h = 1.27$ cm) and tall ($h = 2.54$ cm) wedges with various contact areas ($a = 0.05$, 0.10, 0.20, and 0.40 cm), respectively.

We should recall at this point that an ideal transfer function is represented by a uniformly flat curve for all frequencies. Since it is practically not possible to achieve this goal, we should admit that we can use only a limited range of frequencies within which the transfer function is reasonably

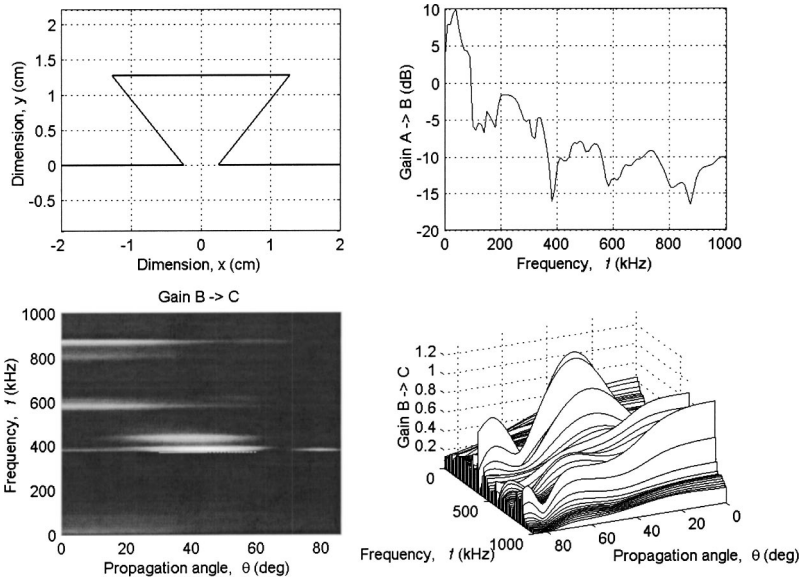

FIG. 7. Design 4. When the wedge–specimen contact area is too large, it causes undesirable aperture effects.

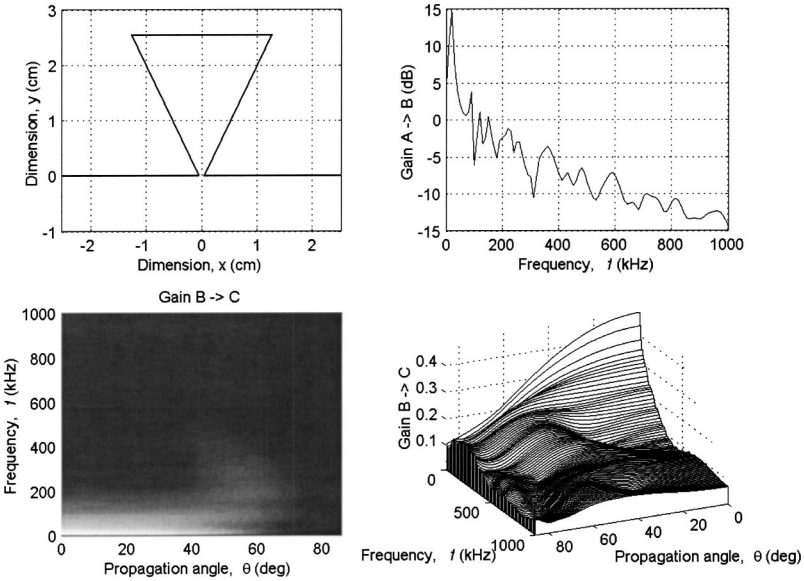

FIG. 8. Design 5. A taller linear wedge with medium contact area provides improved response in both directivity and frequency. Design 6 (graphics omitted). A taller wedge provides excellent response in terms of both frequency and directivity.

flat. Our immediate conclusion upon investigating Fig. 4 is that the base contact area a has little influence on the frequency response of the wedge. We may note that the useful frequency range in this configuration is the band above 500 kHz, where the response function is smooth and flat as compared to that in the low-frequency region. It can also be observed that increasing the base contact area extends the lower bound of the usable frequency band. This trend is particularly strong for the case $h=2.54$ cm, as shown by the extended plateau of smoother and slower slope in the response function for $a=0.40$ cm and $h=2.54$ cm.

B. Transfer functions and directivity

For proper transducer design, it is important to understand the behavior of the emitted wave field that can be characterized quantitatively by the natural focal length N and the aperture angle γ given by the relationship[12]

$$N=\frac{(0.97w)^2 f}{4c_p} \quad \text{and} \quad \sin\gamma=\frac{0.51c_p}{0.97wf}, \tag{12}$$

where c_p is the phase velocity in the specimen and f is the frequency. It can be easily shown from this relationship that the reduced source area decreases N as γ increases. As mentioned earlier, the purpose of using a wedge is to provide a quasipoint (or hairline) source. This means that we intended to generate cylindrical (for hairline sources) or spherical waves (for point sources). To validate the performance in achieving this goal, it is necessary to investigate the directional dependency of the propagating beam. In this paper, we study the directivity of the beam emitted from a transducer–wedge block using the model shown in Fig. 3(b). Directivity is obtained by computing the farfield displacements along an arc located at a fixed distance from the source (we use $w/2=1.27$ cm).

We considered thirteen different wedge shapes in our study. The most common and easiest shape is trapezoid (linear profile). In addition to this simple shape with some variations, we also considered different geometric profiles such as circular, elliptical, and logarithmic shapes. The detailed design specifications are shown in Table II and the cross-

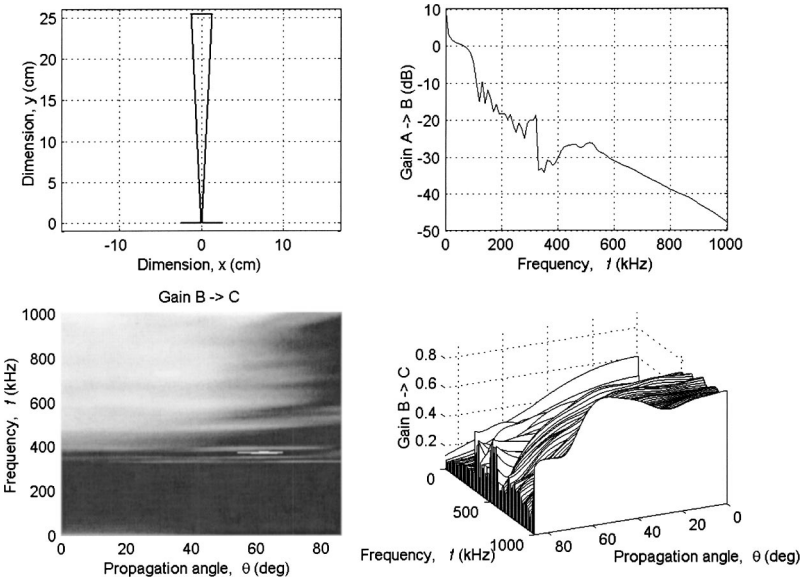

FIG. 9. Design 7. An extremely tall wedge causes instabilities due to excessive attenuation (-40 dB $A-B$) at high frequencies. Design 8 (graphics omitted). Choosing a 45° wall angle does not necessarily produce any improvement. Design 9 (graphics omitted). The frequency and directivity responses of a horn-like wedge are similar to those of Design 5, but it provides a worse gain $A-B$.—Design 10 (graphics omitted). This short horn-like design yields severe instabilities at low frequencies.

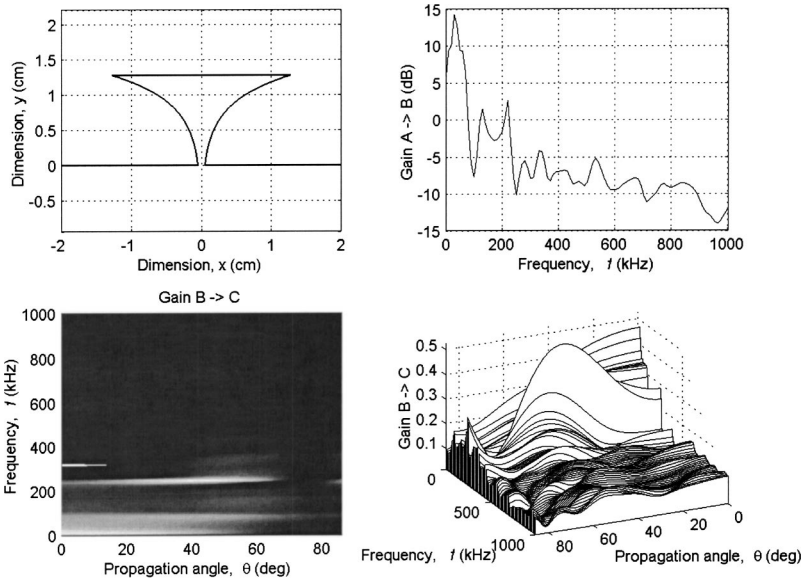

FIG. 10. Design 11. A logarithmic profile does not provide any improvement. Design 12. The performance of a half-circle design is poor.

sectionalviews of each design are illustrated in Figs. 5–10 (in the upper left hand corners of the figures). The curves in the upper right quadrants of these figures represent the frequency-dependent gain produced by the wedge itself for each design, i.e., the ratio of average displacements at the transducer–wedge interface (A) and the wedge-specimen interface (B) plotted as a function of frequency.

The plots at the bottom of Figs. 5–10 are the gains achieved while traveling from a point on B to the arc C. In other words, these figures represent the displacement at a point on C normalized by the average displacement of surface B. The gain between the points on A and C are not shown but they can easily be computed by multiplying the respective gains in paths $A-B$ and $B-C$. The gains at all the discrete points on C are computed and plotted as a function of propagation angle as well as frequency. The same results are displayed both in gray scale images (where the pixel intensity represents the gain) and perspective three-dimensional plots for a clear presentation. Remember that the goal of an ideal design is to achieve a flat platform, which provides little dependency on frequency and propagation angle. Some of the design configurations are omitted in this paper due to space limitations, but they are available by contacting authors. The following are the key observations derived from the set of figures:

Figure 5 (Design 1) shows the results for direct transducer–specimen contact, i.e., no wedge is used in this configuration. The first attempt to reduce the oscillatory performance is to insert a wedge having a very small contact area with the specimen (Design 2, Fig. 6). This certainly enhances the effective aperture angle and gives more uniform gain. But it produces excessive attenuation at some frequencies. Besides, it is difficult manufacture such a sharp wedge. As the wedge–specimen contact area is enlarged (Design 3), the response shows improvements in both frequency and directivity. However, when the area grows excessively (Design 4, Fig. 7), the performance gets worse and great instabilities occur. Up to this point, the best design is No. 3.

Now we play with the wedge height. As the wedge becomes taller (Designs 5 and 6), the directivity is improved and the response becomes smoother, but excessive attenuation at high frequencies makes tall wedges undesirable. Figure 9 (Design 7) shows an unstable response in an extreme case. No revealing relationship was found between the focal depth and the height of the wedge.

Design 8 tests a wedge with a 45° angle in an effort to reduce the effect of reflections inside the wedge, but no improvements are found and the response is very similar to that of Design 3. Horn-like shapes and other geometric variations are tested in Designs 9 to 12. They do not necessarily improve the performance. We also observe that the mechanical coupling due to the presence of the specimen affects the transfer function by attenuating the gain at some frequencies and negatively affecting its behavior. Compare the results of Fig. 4 ($a=0.10$ cm, $h=1.27$ cm) and those of Fig. 10 (Gain

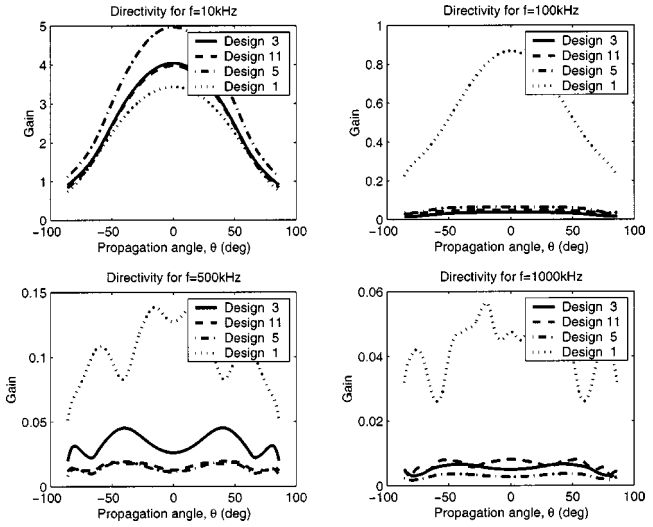

FIG. 11. Directivity plot for some frequencies and selected designs. Design 5 can be chosen as optimal, establishing a compromise between a homogeneous directivity and gain. The enhancements of this design are enlightened against the absence of the wedge (Design 1).

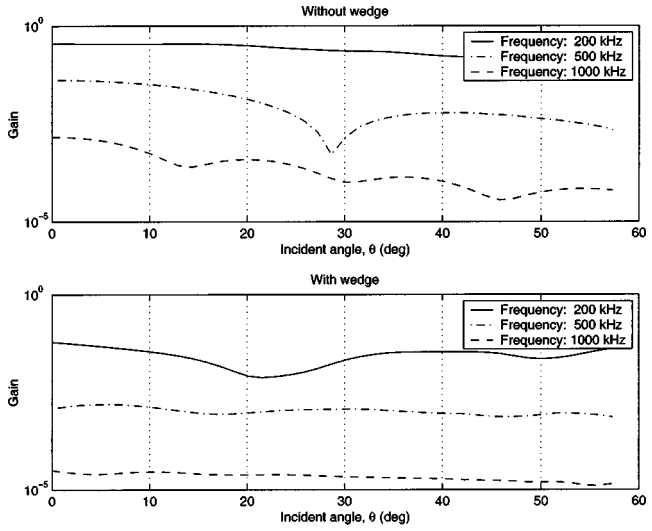

FIG. 12. Response upon inclination of incident wave. Uniformity due to the presence of the wedge is emphasized.

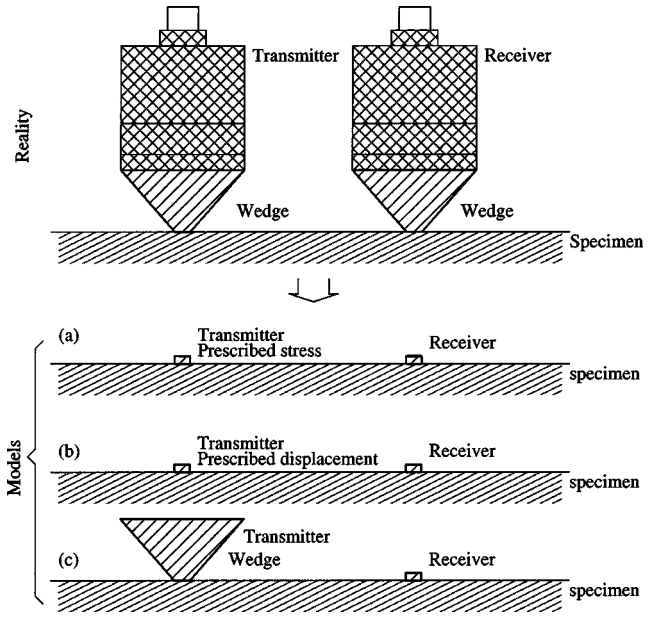

FIG. 13. Model for the study of the boundary conditions at the emitter.

$A-B$). The former takes into account the specimen whereas the latter does not.

We may conclude from these observations that a properly designed wedge can improve the directivity patterns. In order to elucidate the directivity enhancements of the best designs, we show in Fig. 11 the directivities of different designs at various frequencies.

C. Verification of the improvement

The problem of vanishing frequency components due to phase cancellation along the surface measurement can be solved by inserting a wedge. This problem is modeled numerically by considering a semiinfinite space where a plane *P*-wavefront arrives at a variable angle [see Fig. 3(c)].

Figure 12 gives the gain as a function of the incident angle. The cancellation effect is clearly observed from the gain without using the wedge (direct contact). The valleys shown in the gains at frequencies of 500 kHz and 1 MHz are the indication of the phase cancellation effect. These valleys disappear when the wedge is inserted (bottom figure) causing the responses to become more uniform.

D. Boundary conditions

The boundary conditions should take into account the coupling between the transducer and the wedge, which is equivalent to prescribing boundary conditions in terms of stresses and displacements at the transducer–wedge interface and computing the resulting stresses and displacements at the wedge–specimen interface. We can argue here that for a small contact area (point source–receiver), it is sufficient to prescribe the boundary condition at the wedge–specimen interface in terms of either tractions or displacements, which

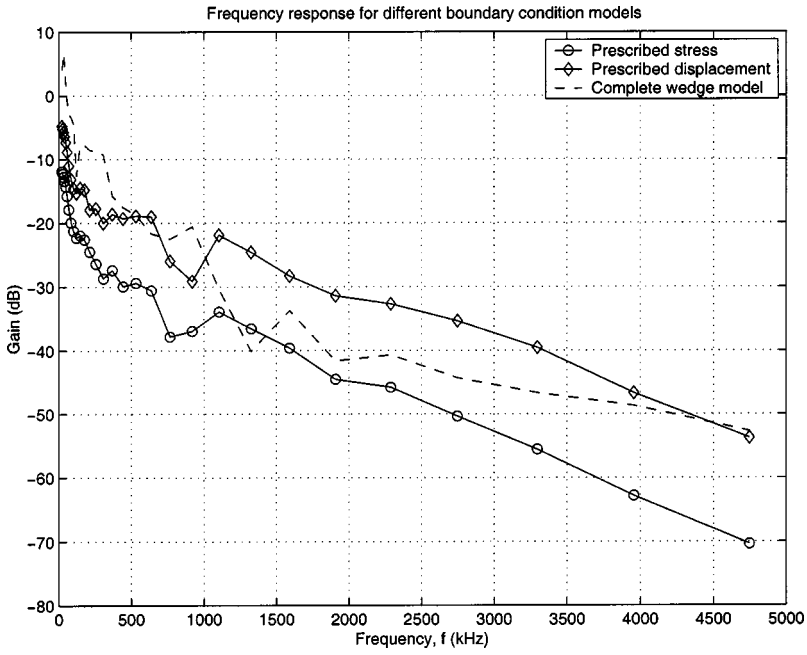

FIG. 14. A comparison of the boundary conditions at the emitter. Prescribed stress and displacements are closely related.

simplifies the modeling of a NDE system and thus reduces the computation time. To prove this, we compare the frequency response of the point source model with that of the complete model whose surface is prescribed either by displacements or by stresses.

Figure 13 shows a NDE setup where transmitting and receiving wedge transducers are placed on the surface of a half space. Figure 14 shows the frequency responses of the output signals due to uniform input. The frequency responses are computed for three different models: (a) the boundary condition of the transmitter is prescribed by uniform stresses; (b) the transmitter boundary condition is prescribed by uniform displacements; and (c) a complete wedge mode. What we can observe in Fig. 14 is that the gains for the three different modes are very similar. The only difference is their scale. This validates our argument that the three models make very little difference in analyzing a wedge-based NDE system. We may choose a simple model that significantly reduces the computation time.

V. CONCLUSIONS

From this study, we obtained conclusions and directions for the effective design of wedge transducers. We also numerically demonstrated their advantages with respect to directivity, frequency responses and computation efficiency.

We obtained a few simple but important guidelines for design, summarized as follows:

- A small contact area improves directivity.
- A higher wedge produces a uniform response for directivity and frequency, but extremely slender wedges suppress high frequency components. A wedge of medium height produces best results.
- Horn-like shapes do not necessarily improve the performance.
- The presence of a well-designed wedge significantly improves the response for the complete range of frequencies.

ACKNOWLEDGMENTS

We would like to gratefully acknowledge the Fulbright Foundation and the Ministerio de Educación Cultura y Deporte for the postdoctoral fellowship FU2002-0442 supporting this work. We would also like to acknowledge the support received by the National Science Foundation (CMS-0218648). We are grateful to Dr. Shih-Chi Liu for his support and encouragement.

[1] W. Sachse, ''Transducer considerations for point-source/point–receiver materials measurements,'' Ultrasonics **25**, 356 (1987).
[2] Y. C. Lee and S. H. Kuo, ''A new point source/point receiver acoustic transducer for surface wave measurement,'' Sens. Actuators, A **94**, 129–135 (2001).
[3] S. Ying, ''Single narrow beam ultrasonic transducer with conical and wedge shaped collimators,'' Ultrasonics **5**, 276 (1967).
[4] T. Imamura, ''Deformation of ultrasonic pulse with diffraction,'' Ultrasonics **37**, 71–78 (1999).
[5] K. Kimoto and S. Hirose, ''A numerical modeling of contact sh-wave transducers,'' in *Review of Progress in Quantitative Nondestructive Evaluation*, edited by D. O. Thompson and D. E. Chimenti (Publisher, City, 2000), Vol. 20.
[6] L. W. Schmerr, *Fundamentals of Ultrasonic Nondestructive Evaluation* (Plenum, New York, 1998).
[7] P. N. Marty, M. J. S. Lowe, and P. Cawley, ''Finite element predictions of guided ultrasonic wave fields generated by piezoelectric transducers,'' in Ref. 5.
[8] S. C. Wooh and Q. Zhou, ''Behavior of laser-induced ultrasonic waves radiated from a wet surface, Part I. Theory,'' J. Appl. Phys. **89**, 3469–3477 (2001).
[9] S. C. Wooh and Q. Zhou, ''Behavior of laser-induced ultrasonic waves radiated from a wet surface, Part II. Experimental work,'' J. Appl. Phys. **89**, 3478–3485 (2001).
[10] S. C. Wooh and Y. J. Shi, ''Synthetic phase tuning of guided waves,'' IEEE Trans. Ultrason. Ferroelectr. Freq. Control **48**, 209–223 (2001).
[11] Y. J. Shi, S. C. Wooh, and M. Orwat, ''Laser-ultrasonic generation of Lamb waves in the reaction force range,'' Ultrasonics **41**, 623–633 (2003).
[12] R. K. Miller, *Nondestructive Testing Handbook*, American Society for Nondestructive Testing, 5th ed. (Publisher, City, 1986), Vol. 5.
[13] G. Rus, ''Numerical methods for nondestructive identification of defects,'' Ph.D. thesis, Universidad de Granada, E.T.S.I. Caminos, C. y P., June 2001. Electronic mail: grus@ugr.es.
[14] J. Domínguez, *Boundary Elements in Dynamics* (Elsevier, New York, 1993).
[15] G. Rus and R. Gallego, ''Optimization algorithms for identification inverse problems with the boundary element method,'' Int. J. Eng. Anal. B.E. **26**, 315–327 (2002).